Effect of chirality on liquid crystals in capillary tubes with parallel and perpendicular anchoring

H.-S. Kitzerow,[1] B. Liu,[2] F. Xu,[2] and P. P. Crooker[2]
[1]*Technische Universität Berlin, Sekr. ER 11 Strasse des 17. Juni 135, 10623 Berlin, Germany*
[2]*Department of Physics and Astronomy, University of Hawaii, 2505 Correa Road, Honolulu, Hawaii 96822*
(Received 26 February 1996)

The director field of a cholesteric liquid crystal confined to cylindrical cavities with parallel and perpendicular surface anchoring was studied by means of optical polarizing microscopy. The chirality of the liquid crystal could be varied continuously due to a temperature-induced twist inversion of the cholesteric structure. The results indicate the occurrence of a twisted escaped radial structure for perpendicular anchoring and an eccentric double twist configuration for parallel anchoring. [S1063-651X(96)09507-4]

PACS number(s): 61.30.Gd, 61.30.Jf

I. INTRODUCTION

Nematic liquid crystals confined to small cylindrical cavities have been extensively studied in the past. The anchoring of the director at the curved surface of capillary tubes leads to three-dimensional director fields that may exhibit characteristic defect structures [1–5]. The anchoring energy [2], the ratio of the elastic coefficients K_{11}/K_{33} [1,3], and even the saddle-splay elastic constant K_{24} [2] have been determined by a detailed analysis of the director field of nematic liquid crystals in cylindrical cavities. However, the director fields of *chiral* liquid crystals in capillary tubes have been much less investigated.

Nonchiral nematic liquid crystals are characterized by a uniform director field. However, the addition of chiral molecules causes a twisted director field known as the cholesteric phase. Williams and Bouligand [6], Cladis, White, and Brinkman [7], and Lequeux and Kléman [8,9] have found various helicoidal structures for cholesteric liquid crystals confined to a capillary with perpendicular anchoring. More recently, Ondris-Crawford *et al.* [10] have detected a pitch-induced transition from a radially twisted to an axially twisted structure in submicrometer cavities with concentric anchoring.

In the present paper, we report on the behavior of an induced cholesteric mixture confined to glass capillaries with well-defined perpendicular or parallel anchoring. Induced cholesteric mixtures consist of a nematic host and a small amount of a chiral dopant. For many systems of this kind, the reciprocal value of the pitch p is proportional to the concentration c of the chiral component: $p^{-1}=hc$, where h is the helical twisting power. In the experiments presented here we have used a chiral dopant for which h is temperature dependent and indeed shows a sign inversion at a particular temperature T_{inv}, i.e., the handedness of the helix in the temperature range below T_{inv} is opposite the handedness above T_{inv}. At T_{inv}, the absolute value of the pitch diverges. This feature enables us to vary the cholesteric pitch p over a large range by simply adjusting the temperature. Since the twist inversion occurs at a temperature far away from any phase transition, we expect the elastic coefficients to be nearly temperature independent, in contrast to the system studied by Cladis, White, and Brinkman [7].

For both parallel and perpendicular anchoring, transitions from a typical nematic structure (at which p is infinite) to complicated spiral patterns (for which p is less than the capillary diameter) are observed. For perpendicular anchoring there is a transition from the escaped radial structure to a twisted escaped radial structure, while for parallel anchoring there is a transition from uniform alignment to a double twist cylinder configuration [11]. These structures differ from previously observed vector fields [7] and are discussed with respect to recent theoretical predictions [12].

II. EXPERIMENT

The liquid crystals used in our experiments are chiral multicomponent mixtures that exhibit the cholesteric phase (N^*) in a broad temperature range. The helical structure of the N^* phase shows a very strong temperature dependence of the pitch and an inversion of the handedness at a temperature T_{inv} within the cholesteric temperature range. This temperature dependence of the pitch enables us to study the effects of chirality on the director fields by simply varying the temperature.

In order to obtain such mixtures, we used nematic host mixtures with broad nematic temperature ranges, such as ZLI-2806 (negative dielectric anisotropy) or ZLI-1840 (positive dielectric anisotropy), both from E. Merck. The cholesteric phase was induced by adding the chiral dopants D13

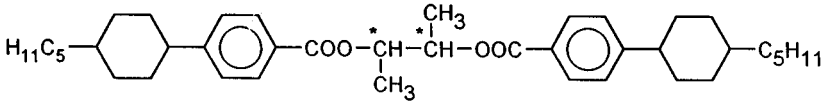

and D112

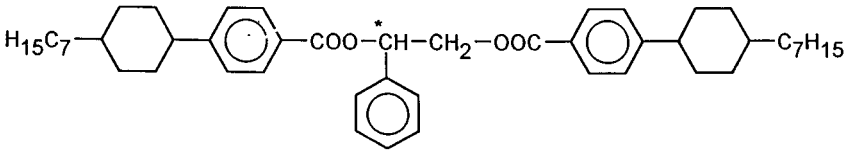

to the nematic host mixture. Both components were synthesized in our laboratory. The helical twisting power of D13 depends very strongly on temperature, causing a right-handed helical structure at low temperatures and a left-handed helical structure at high temperatures [13]. The sign inversion of the pitch induced by this compound in ZLI-2806 was found to occur at $T_{\mathrm{inv}}=101.3$ °C (Fig. 1). To reduce the inversion temperature and bring both right- and left-handed regimes into the N^* temperature range we added D112, which is known to exhibit a very high, temperature-independent helical twisting power [14]. Thus the addition of D112 to a mixture of D13 and ZLI-2806 shifted T_{inv} (Fig. 1) without affecting the slope of $p^{-1}(T)$. The dependence of the temperature of the helix inversion T_{inv} on the weight fraction x_{D112} of D112 is approximately described by the linear relation $T_{\mathrm{inv}}=a+bx_{\mathrm{D112}}$, where $a=101.3$ °C and $b=-1.498\times10^4$ °C.

The results presented in this paper were obtained for two very similar mixtures: *mixture A*, 2.5% D13, 0.3% D112, 97.2% ZLI-2806 ($T_{\mathrm{inv}}=41.5$ °C), and *mixture B*, 2.9% D13, 0.4% D112, 96.7% ZLI-2806 ($T_{\mathrm{inv}}=55.6$ °C), which were used for the samples with perpendicular and parallel anchoring, respectively.

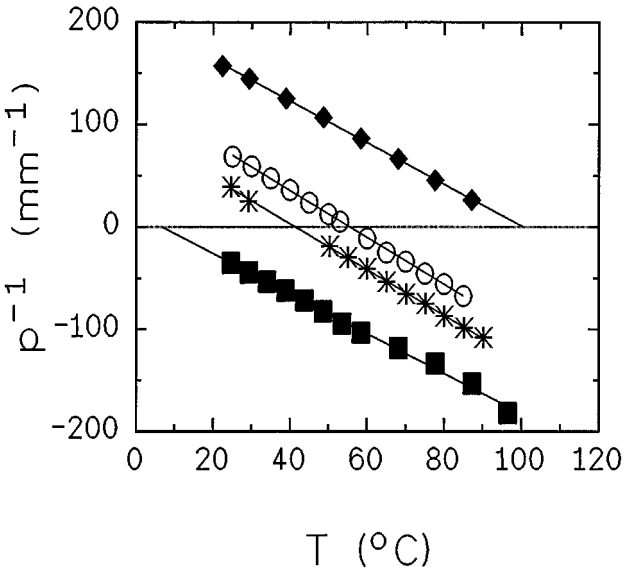

FIG. 1. Inverse pitch versus temperature for mixtures with different concentration of the chiral dopants D13 and D112 in the nematic host ZLI-2806. ♦, 2.45% compound D13, 97.55% ZLI-2806; ∗, 2.50% compound D13, 0.36% compound D112, 97.14% ZLI-2806 (mixture *A*); ○, 2.92% compound D13, 0.36% compound D112, 96.72% ZLI-2806 (mixture *B*); ■, 2.50% compound D13, 0.62% compound D112, 96.89% ZLI-2806.

Glass capillary tubes with diameters of 25, 50, 75, 100, and 200 μm were treated in order to obtain suitable surface anchoring and then filled with the liquid crystal. In order to achieve *perpendicular anchoring* of the director at the liquid-crystal–glass interface, the capillaries were filled with a solution of lecithin and the solvent was allowed to evaporate before the capillary was filled with the liquid crystal. To achieve *parallel anchoring*, the inner surface was treated with an anisotropic polymer film formed by photoinduced cross linking with polarized light (known as the LPP effect in [15]). For the latter purpose, poly(vinyl 4-methoxycinnamate) (PVMC) was deposited on the glass surface and an anisotropic polymer film was formed by illuminating the rotating capillary with linearly polarized UV light ($I\approx11$ mW/cm^2) from a 400-W halogen lamp (Fig. 2). The anchoring orientation of the director is known to be perpendicular to the plane of polarization of the UV radiation used for the curing process [15]. Thus the orientation of the plane of polarization perpendicular to the cylinder axis resulted in a uniform anchoring of the director along the cylinder axis.

In order to determine the director fields, the cylinders were placed between crossed polarizers in a microscope and photographed in the transmission mode using monochromatic light and several polarizer configurations. Guided by these pictures, a model for the director configuration was proposed and the transmission pattern calculated. The computer program for the transmission pattern determines the absorption and phase shift of the polarization components of the light beam as it passes through the polarizer, multiple slices of the droplet director field, and finally through the analyzer. Details of the calculation, which uses the Mueller-Stokes formalism, are given by Xu, Kitzerow, and Crooker [16]. Finally, the calculated patterns were compared with the measured patterns and the model refined. This process was repeated until the calculated patterns were in agreement with the experimental observations.

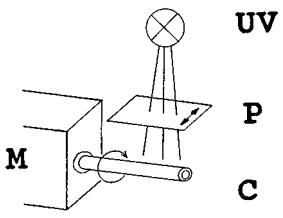

FIG. 2. (a) Experimental setup surface preparation using the LPP effect. UV, UV light source; P, polarizer; M, stepping motor; C, capillary tube coated with poly-(vinyl 4-methoxy-cinnamate), PVMC.

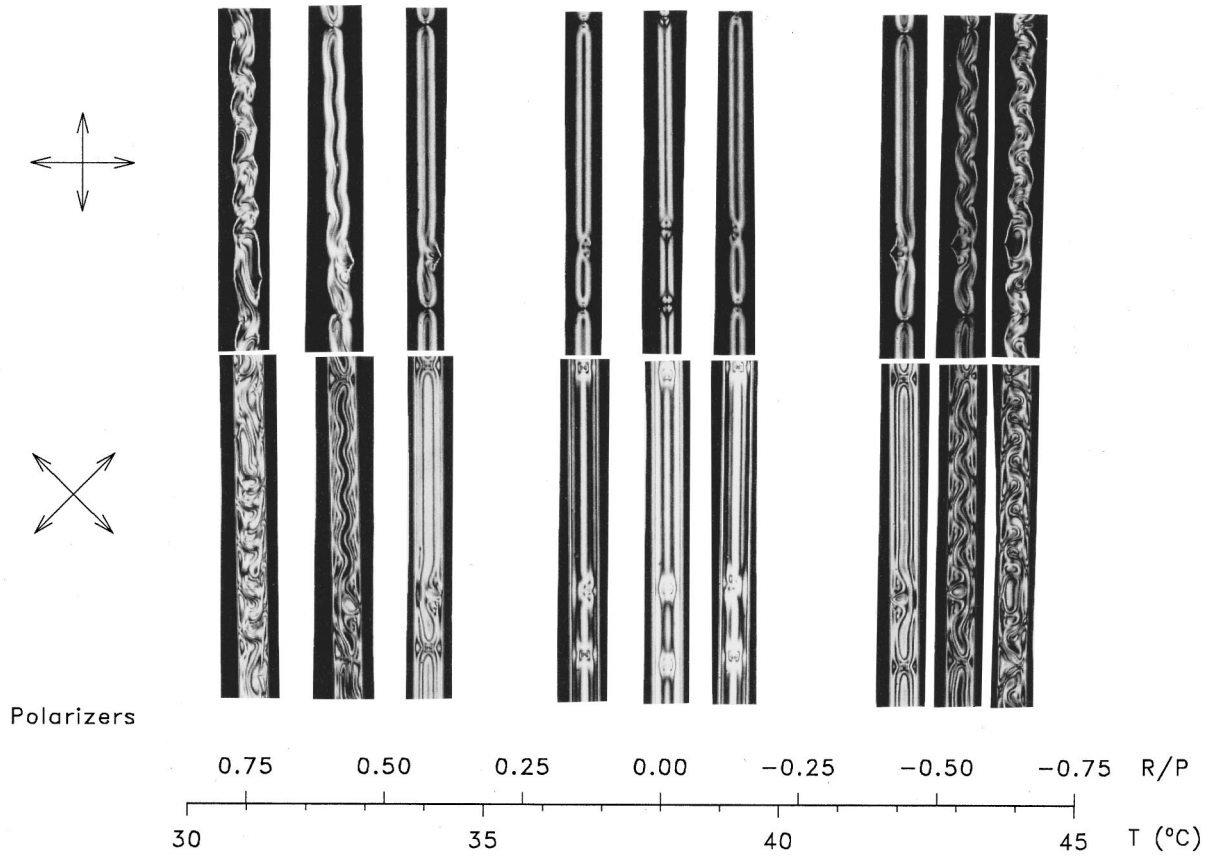

FIG. 3. Evolution of the director configuration in a capillary as a function of tube radius R over pitch P. The microscope photographs are all of one capillary and are positioned over the corresponding bulk R/P ratios. Arrows at the left show the arrangement of crossed polarizers for each row. $1/P$ is linearly related to the temperature as shown on the temperature scale. Note the behavior of the point defects and the onset of the helical instability.

III. RESULTS

A. Perpendicular anchoring

The textures for cylinders with perpendicular anchoring are shown in Fig. 3. The horizontal axis shows the ratio R/p, where R is the capillary radius and p is intrinsic pitch; this ratio is proportional to the chirality $1/p$. Since $1/p$ is linearly related to the temperature T, the temperature is also shown. The microscope photographs are all of the same sample and are positioned over their respective temperatures. Two crossed-polarizer alignments are shown: in the upper row the polarizer axes are aligned parallel and perpendicular to the tube axis; in the lower row they are aligned at $\pm 45°$ to the tube axis. Note that in the vicinity of zero chirality ($T_{\mathrm{inv}}=38.0$ °C) the texture exhibits straight sections where the director configuration is constant along z, and point defects where the director is undefined. The point defects are either hedgehog defects (radial point defects, or monopoles) or hyperbolic defects (antimonopoles).

As the chirality increases from zero, the straight sections appear to change gradually, until at $R/p \approx 0.5$ they become unstable and take on a sinusoidal appearance. The amplitude of this sinusoidal pattern increases rapidly with further increasing chirality, becoming nonsinusoidal but still periodic at higher chiralities. Eventually the texture becomes chaotic. Note also that the optical textures are somewhat different at corresponding left-and right-handed chiralities; this effect is attributed to the temperature variation of the elastic constant ratios.

The two types of defects are affected differently by chirality. At zero chirality, both types of point defects lie on the cylinder axis. As the chirality increases, the hyperbolic defect remains on the axis, but the hedgehog defect becomes displaced toward the cylinder wall. For opposite chirality, the hedgehog defect moves in the opposite direction.

Studies were made using capillaries with diameters of 25, 50, 75, and 100 μm; the collective behavior can be qualitatively separated into regions depending on the pitch p and capillary diameter D, as shown in Fig. 4(a). In the *nematic-like* region [region (N)] the pattern changes little from the pure nematic (zero chirality) case. In the *displaced hedgehog defect* region [region (D)] the hedgehog defect is displaced toward the wall, while in the *surface defect* region [region (C)] the defect has reached the wall. Finally, in the *spiral* region, the straight lines take on a spiral or helical structure. If the anchoring is strong (no tilt of the director away from the perpendicular direction at the boundary), the capillary diameter D and pitch p are the only two lengths in the problem and the behavior should only depend on their ratio. The lines in Fig. 4(a) are best fits to the equation $p^1 = C/D$, where C is a constant; within our ability to determine the region boundaries, the fits are acceptable. Figure 4(b) shows the same data plotted as the ratio D/p against D; again,

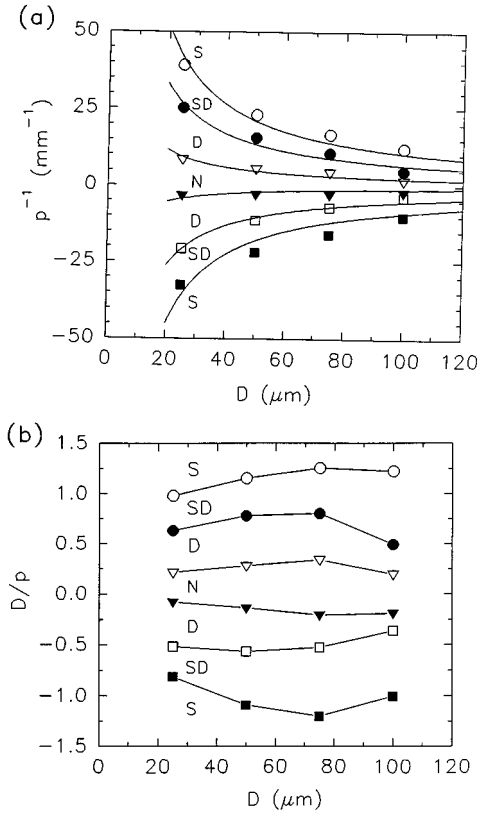

FIG. 4. Stability regions for capillaries of different radii. (a) p^{-1} vs D. N, nematiclike; D, displaced hedgehog defect; SD, surface defect; S spiral. Lines are best fits to $p^{-1}=\text{const}/D$. (b) R/p vs D. Lines are guides to the eye.

within our ability to determine the boundaries, D/p is indeed independent of the diameter, as expected.

We have been able to determine the director configurations of the straight sections, which change only slowly with increasing chirality. Let the position of the director be specified by cylindrical coordinates (ρ,ϕ,z) and the director orientation be given by two angles β and γ as shown in the inset to Fig. 6. β, the angle between the director and the radial direction, describes the director tilt in the meridional plane. γ, the angle between the projection of the director on a plane perpendicular to the radial axis and the z axis, describes the twist about any radius. In the nonspiral regions these angles are functions of ρ only, so that in cylindrical coordinates the director takes on the form

$$\hat{\mathbf{n}}(\rho)=\hat{\boldsymbol{\rho}}\cos\beta-\hat{\boldsymbol{\phi}}\sin\beta\sin\gamma-\hat{\mathbf{z}}\sin\beta\cos\gamma. \qquad (1)$$

Our task is therefore to determine $\beta(\rho)$ and $\gamma(\rho)$.

We have assumed that $\beta(\rho)$ and $\gamma(\rho)$ have the polynomial form $\Sigma a_n\rho^n$ and have retained only the minimum number of coefficients required to explain the data. Along the z axis, $\beta(0)=\pi/2$ and $\gamma(0)=0$; at the boundary, $\beta(\rho_o)=0$ and $\gamma(\rho_o)$ can be left unspecified. Subject to these constraints, the coefficients are then chosen to construct model director configurations that best agree with experiment.

The comparison with experiment was accomplished by first assuming values for the polynomial coefficients for $\beta(\rho)$ and $\gamma(\rho)$ and calculating the transmitted intensity patterns as described previously. The calculated patterns were then compared with the measured patterns and the model refined until the calculated and measured patterns agreed.

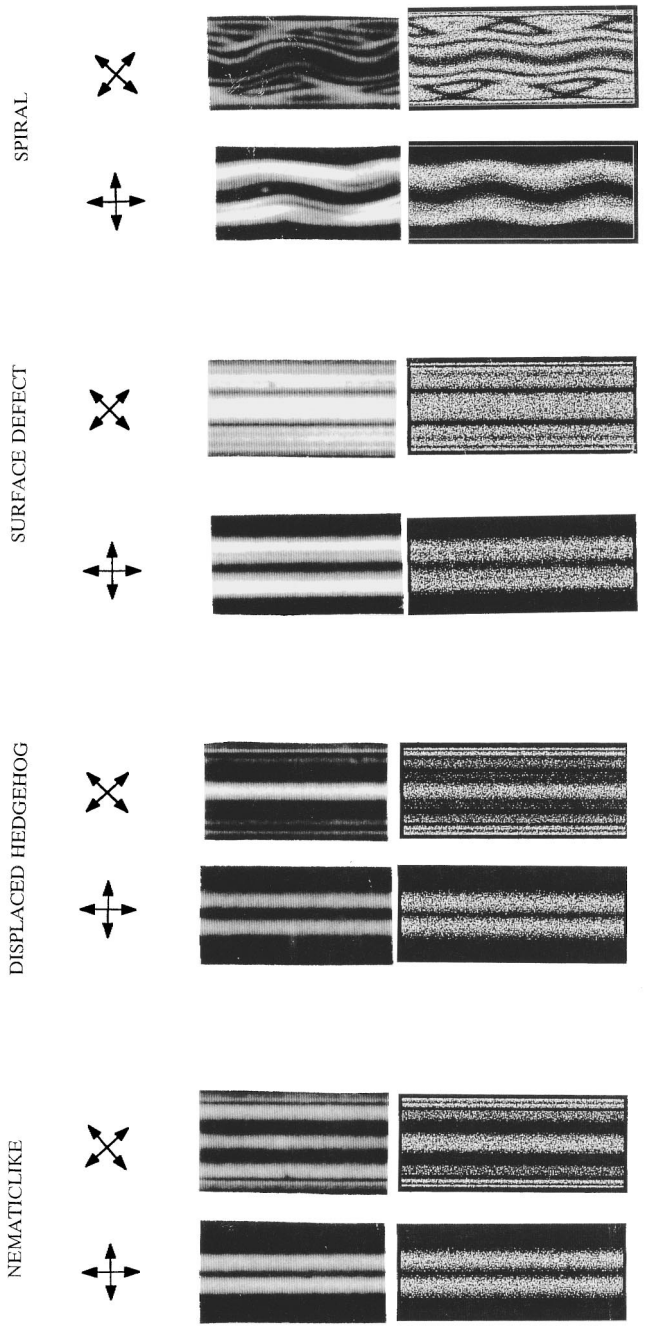

FIG. 5. Observations and calculated director patterns. Left column: microscope photographs with polarizer angles denoted by arrows. Right column: model transmission patterns.

Figures 5 and 6 show our results. The pictures on the left in Fig. 5 are microscope photographs; those on the right are the calculated transmission patterns. The polynomials utilized for each fit are shown in the graphs for β and γ of Fig. 6. As prescribed by the boundary conditions, $\beta(\rho)$ proceeds smoothly from the axial direction at the center to the radial direction at the boundary; except for an increased persistance in maintaining its axial orientation near the center, its behavior is unremarkable. $\gamma(\rho)$, on the other hand, describes the twist; the slope $d\gamma/d\rho$ is in fact proportional to the chirality. From the graph it can be seen that $\gamma(\rho)$ increases steadily at

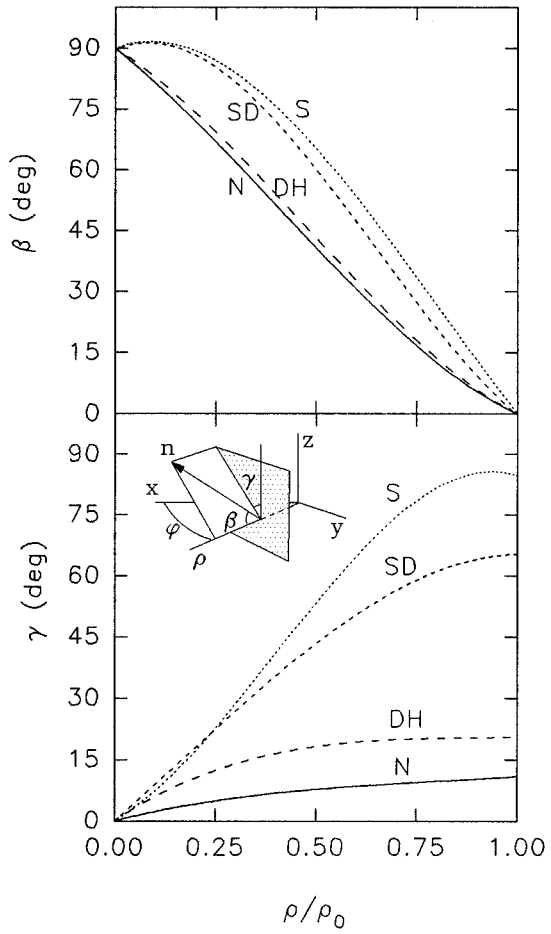

FIG. 6. Variation of director angles β and γ with cylinder radius ρ in the various stability regions. N, nematic; D, displaced hedgehog defect; SD, surface defects; S, spiral. See the text for an interpretation of the graphs in the spiral region. Inset: definition of β and γ.

the center as the bulk chirality increases and levels off near the edge where β approaches 0 and γ becomes less meaningful. The twist is therefore manifested in an increased radial twist.

As the chirality increases through the value at which the chiral instability occurs, the instability is manifested by the center of the axially symmetric director configuration becoming slightly offset from the cylinder axis, spiraling around the axis in the z direction. The rest of the director pattern is correspondingly stretched, compressed, or sheared so that the original boundary conditions are preserved. This situation requires that a special interpretation be given to the graphs for β and γ in the spiral region, namely, that $\rho/\rho_0=0$ corresponds to the center of the offset pattern and $\rho/\rho_0=1$ corresponds to the boundary, regardless of the direction in which ρ is taken.

For larger chirality, the distortion becomes nonsinusoidal, but still periodic. The director configuration in this higher-order regime is very complex and we have not attempted any fits.

B. Parallel anchoring

For cylinders with *parallel* anchoring, the cholesteric textures observed on heating the sample are shown in Fig. 7.

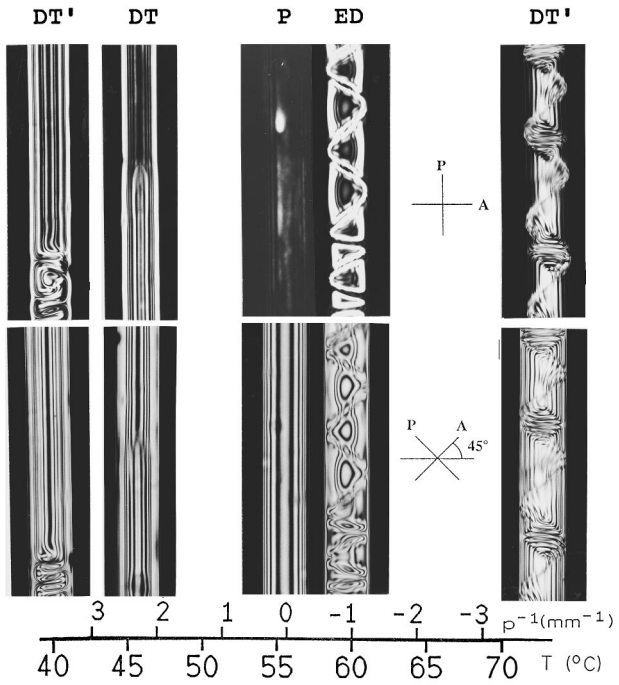

FIG. 7. Transmission pattern of cholesteric cylinders with parallel anchoring between crossed polarizers (mixture *B*). For the temperature dependence of the intrinsic pitch see Fig. 1.

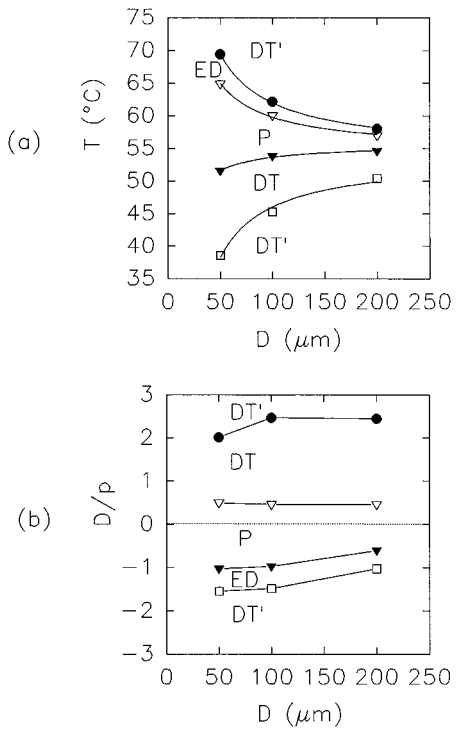

FIG. 8. Stability diagrams for structures with parallel anchoring. (a) Stability regions denoted by temperature for various tube diameters D. DT, double twist, DT′, irregular double twist; ED, eccentric double twist; P, parallel. (b) The same stability diagram, using the reduced unit D/p instead of T.

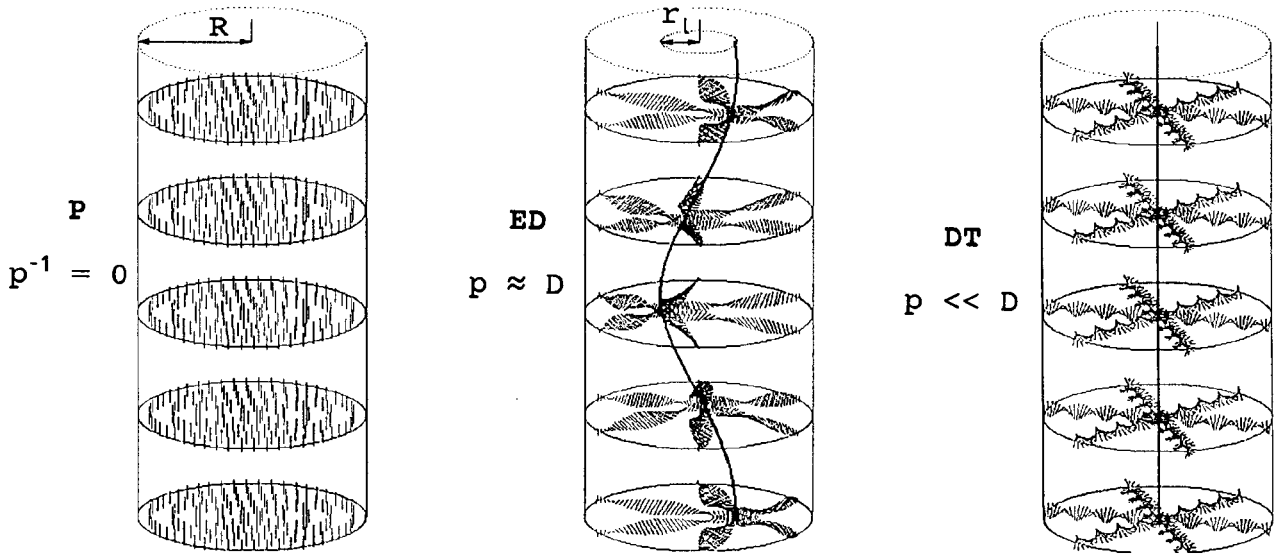

FIG. 9. Model structures to explain the observed transmission for different chiralities. P, uniform parallel director field; ED, eccentric double twist cylinder; DT, double twist cylinder.

The corresponding stability diagram is shown in Fig. 8. As in the case of perpendicular anchoring, we again see that patterns for capillaries of different radii depend only on the ratio D/p. Beginning at the lowest temperature ($T<T_{\mathrm{inv}}$), where the pitch is much smaller than the diameter D of the cylinder, observation of the sample between crossed polarizers reveals straight bright and dark lines parallel to the cylinder axis. This pattern can be explained by a director field where the pitch axes lie along the cylinder radii and the director lies in the ϕ-z plane (Fig. 9). Using the coordinates defined in Fig. 6 and Eq. (1), $\beta=\pi/2$ everywhere and $\gamma=2\pi\rho/p^*$. As we shall see, p^* is not the bulk pitch.

It is interesting to note that tubes with the same helical arrangement are considered to be the basic unit of the structure of blue phases [11]. In agreement with these earlier considerations, we call this the *double twist* (DT) structure. The dark and bright lines seen in the polarizing microscope can be identified as the ''fingerprint'' lines, separated by distance $p^*/2$, as are commonly seen in cholesteric liquid crystals. When the pitch is very small, $|p|<D/2$, the double twist cylinder is not perfect and the fingerprint lines show some loops. The helicoidal instability leading to these loops has been discussed earlier by Lequeux and Kléman [9]. In the stability diagram (Fig. 8) we denote this *irregular double twist* structure as DT′. The loops disappear on increasing temperature so that a perfect DT structure is observed in the range $D/2<|p|<2D$.

As expected, the distance between the fingerprint lines increases with increasing pitch when the temperature approaches the value T_{inv}. The variation of this distance with chirality is not continuous, however, but occurs in a steplike way. Due to the anchoring at the cylinder surface, the pitch p^* may differ from the intrinsic pitch p, since it obeys the boundary condition $mp^*=D$, where m is an integer. As a consequence, the fingerprint lines disappear pair by pair on approaching T_{inv} and the disappearance of each pair of lines is connected to the movement of a dislocation along the cylinder axis through the entire cylinder.

Close to the inversion temperature T_{inv} where the intrinsic pitch p is larger than the tube diameter, the director is uniformly aligned parallel to the cylinder axis (Fig. 9). This *parallel* structure (P) appears completely dark if the polarizer and analyzer are parallel and perpendicular to the cylinder axis; however, bright and dark lines appear when the polarizers are tilted at $\pm 45°$ to the cylinder axis. In contrast to the fingerprint lines, these lines, which occur for $T\approx T_{\mathrm{inv}}$ are due to the birefringence of the uniaxial nematic liquid crystal. The transmitted intensity for the sample between polarizers crossed at $\pm 45°$ to the cylinder axis is

$$I=\frac{1}{2}\,I_0\,\sin^2\left[\frac{\pi\Delta n\sqrt{D^2-4\rho^2}}{\lambda}\right], \tag{2}$$

where ρ is the radial distance from the tube axis and $(D^2-4\rho^2)^{1/2}$ is the effective thickness of the birefringent tube. In agreement with Eq. (2), the distances between the dark and bright lines observed for $T\approx T_{\mathrm{inv}}$ decrease with increasing distance ρ from the tube axis. This separation differs from that of the fingerprint lines described above, since the latter are separated by a constant distance.

If the temperature is further increased beyond the P region, the chirality of the liquid crystal changes handedness and the pitch decreases with increasing temperature. In the region where $\frac{2}{3}D<|p|<D$, which we call the *eccentric double twist* (ED) region, a complicated but very regular spiral pattern develops. In order to explain the spiral we assume a director configuration of the form

$$\hat{\mathbf{n}}(\rho_1)=\hat{\boldsymbol{\phi}}_1-\sin_1+\hat{\mathbf{z}}\,\cos\gamma_1, \tag{3}$$

where $\hat{\boldsymbol{\rho}}_1$, $\hat{\boldsymbol{\phi}}_1$, and $\hat{\mathbf{z}}$ are unit vectors in cylindrical coordinates relative to a new origin at (x_1,y_1,z), which lies on the offset twist axis. The twist $\gamma_1=2\pi\rho_1/p$ and radial distance $\rho_1=[(x-x_1)^2+(y-y_1)^2]^{1/2}$ are for a particular point relative to this origin, through which passes a nonsingular disclination line. This disclination line forms a spiral with amplitude r_1 and pitch P, i.e., $x_1(z)=r_1\cos(2\pi z/P)$ and $y_1(z)=r_1\sin(2\pi z/P)$.

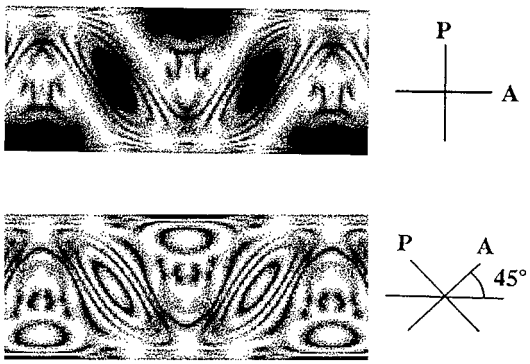

FIG. 10. Calculated transmission for the ED structure, as described by Eq. (3) with $D=100$ μm, $r_1=50$ μm, and $P=200$ μm.

The structure described by Eq. (3) is characterized by a planar anchoring of the director at the cylinder surface, i.e., $\beta(\rho_0)=\pi/2$. However, the azimuthal anchoring angle γ in Eq. (3) does not coincide with the anchoring direction $\gamma=0$ prescribed by the orientation of the anisotropic polymer film at the boundary. We propose, on the basis of the experimental evidence given below, that the anchoring energy W_φ is weak enough to be overcome by the director torques. This proposal is in agreement with recent measurements on photoinduced anisotropic polymer films [17], which indicate that W_φ for PVMC is an order of magnitude smaller than that for rubbed polyimide [17].

The calculation of the transmitted intensity of the ED model is shown in Fig. 10. This figure is in good qualitative agreement with the experimental observation if we set $r_1=D/2$, i.e., if the nonsingular disclination line is located at the surface of the cylinder. When focusing on different planes of the sample, the pattern observed for crossed polarizers oriented parallel and perpendicular to the axis confirms the presence of a bright spiral at the surface of the cylinder. This disclination line is nonsingular: unlike typical singular disclination lines, the spiral is characterized by a smooth variation of the light intensity, which indicates a strong but continuous variation of the director field in its vicinity.

On further increasing of the temperature, parallel fingerprint lines interrupted by loops appear again, indicating a double twist structure DT′. If the sample is maintained at constant temperature, these loops eventually disappear and a perfect DT structure is formed. It is interesting to note that the appearance of the different structures depends on the history of the sample. Unlike the stability diagram for perpendicular anchoring (Fig. 4), the stability diagram for parallel anchoring (Fig. 8) is not symmetrical with respect to $D/p=0$. If the sample is allowed to relax to the perfect DT structure at high temperature and then cooled, the sequence of structures in the phase diagram of Fig. 8 is reversed. That is, whether heating or cooling we observe the same sequence of phases DT′-DT-P-ED-DT′.

IV. CONCLUSION

Our investigations on cholesteric liquid crystals in cylinders with perpendicular and parallel anchoring reveal the appearance of various chiral structures in addition to the director fields observed previously. For perpendicular anchoring, our system differs completely from the earlier observation on a mixture of cholesteryl-nonanoate and *p*-cyanobenzylidene-*p*′-octyloxyaniline by Cladis, White, and Brinkman [7]. In that system, the proximity of the cholesteric–smectic-*A* phase transition caused both the pitch and the ratios of the elastic coefficients K_{33}/K_{11} and K_{22}/K_{11} to diverge as the transition was approached. Below the transition, in the smectic-*A* phase, a planar radial structure was observed [7], which is characterized by a singular disclination line with strength $s=1$ in the center of the tube. Above the transition, in the cholesteric phase, a splitting of this defect line into one $s=2$ line and two $s=\frac{1}{2}$ lines was found [7].

In contrast, our system with perpendicular anchoring does not show a defect line but rather an escaped radial (ER) structure with *point defects* for $p^{-1}=0$. This structure is brought about by changing chirality alone; the ratio of the elastic coefficients in our system is not expected to vary much with temperature or chirality since no phase transition is involved. Furthermore, the additional motion of the hedgehog defect toward the surface is an effect driven by chirality alone. A similar transformation from a volume defect to a surface defect has been observed in nematic droplets under the influence of an electric field [16] and is in agreement with the topological considerations by Volovik and Lavrentovich [18]. On the other hand, the *hyperbolic* defects in our system are stable volume defects. This is reasonable: it is impossible to satisfy the perpendicular boundary conditions with a hyperbolic defect.

Small intrinsic pitch ($p<D$) leads to a twisted ER structure, in contrast to the theoretical considerations of Bezić and Žumer [12], who assumed two-dimensional director fields with a pitch axis along the cylinder axis. Escaped radial structures therefore have to be considered for a cholesteric liquid crystal confined to a cylinder. [19] Although our observations differ considerably from the results of Cladis, White, and Brinkman [7], they confirm the expectation that the sum of the disclination strengths is constant.

For *parallel anchoring* (Figs. 7–10), we observed uniform parallel alignment in the nematic phase and double twist cylinders with a radial arrangement of the pitch axes for the highly twisted liquid crystal. In the intermediate range $p\approx D$, our observations fit an eccentric double twist model. A similar structure with a displaced ($s=1$) χ-disclination line, but with concentric anchoring was proposed by Bezić and Žumer [12]. The double twist configuration DT occurring for small pitch is identical to the *radially twisted axial* structure observed in submicron cavities with concentric anchoring [10]. However, our system with parallel anchoring does not show a discontinuous transition from an axially twisted to the radially twisted structure (as reported in Ref. [10]) but rather a continuous transition from the uniform planar structure to the radially twisted structure through the metastable eccentric double twist configuration. We conclude that the twist axis of the cholesteric director field in cylindrical confinement may not be oriented parallel or perpendicular to the cylinder axis. More complicated double twist structures, such as our ED model, may also have to be considered.

ACKNOWLEDGMENTS

H.K. would like to thank Professor V. Chigrinov for providing the polymer-precursor PVMC that was used to achieve planar anchoring at the glass–liquid-crystal interface of the capillaries, and Dr. F. Oestreicher for supplying the chiral dopants D13 and D112. This work was supported by the Deutsche Forschungsgemeinschaft (Grant No. Sfb 335) and the Volkswagenstiftung (Grant No. I/70362).

[1] P. E. Cladis and M. Kléman, J. Phys. (Paris) **33**, 591 (1972).
[2] G. P. Crawford, D. W. Allender, J. W. Doane, M. Vilfan, and I. Vilfan, Phys. Rev. A **44**, 2570 (1991).
[3] G. P. Crawford, J. A. Micheltree, E. P. Boyko, W. Fritz, S. Žumer, and J. W. Doane, Appl. Phys. Lett. **60**, 3226 (1992).
[4] R. J. Ondris-Crawford, G. P. Crawford, J. W. Doane, S. Žumer, M. Vilfan, and I. Vilfan, Phys. Rev. E **48**, 1998 (1993).
[5] R. J. Ondris-Crawford, G. P. Crawford, S. Žumer, and J. W. Doane, Phys. Rev. Lett. **70**, 194 (1993).
[6] C. Williams and Y. Bouligand, J. Phys. (Paris) **35**, 589 (1974).
[7] P. E. Cladis, A. E. White, and W. F. Brinkman, J. Phys. (Paris) **40**, 325 (1979).
[8] F. Lequeux, C. R. Acad. Sci. Paris, Ser. II **303** (9), 765 (1986).
[9] F. Lequeux and M. Kléman, J. Phys. (Paris) **49**, 845 (1988).
[10] R. J. Ondris-Crawford, M. Ambrožič, J. W. Doane, and S. Žumer, Phys. Rev. E **50**, 4773 (1994).
[11] J. P. Sethna, Phys. Rev. B **31**, 6278 (1985).
[12] J. Bezić and S. Žumer, Liq. Cryst. **14**, 1695 (1993).
[13] G. Heppke, D. Lötzsch, and F. Oestreicher, Z. Naturforsch. Teil A **42**, 279 (1987).
[14] G. Heppke, D. Lötzsch, and F. Oestreicher, Z. Naturforsch. Teil A **41**, 1214 (1986).
[15] M. Schadt, K. Schmitt, V. Kozinkov, and V. Chigrinov, Jpn. J. Appl. Phys. **31**, 2155 (1992).
[16] F. Xu, H.-S. Kitzerow, and P. P. Crooker, Phys. Rev. A **46**, 6535 (1992).
[17] V. P. Vorflusev, H.-S. Kitzerow, and V. G. Chigrinov, Jpn. J. Appl. Phys. **34**, L1137 (1995).
[18] G. E. Volovik and O. D. Lavrentovich, Zh. Eksp. Teor. Fiz. **85**, 1997 (1983) [Sov. Phys. JETP **58**, 1159 (1984)].
[19] S. Kralj and S. Žumer, Liq. Crys. **15**, 521 (1993).